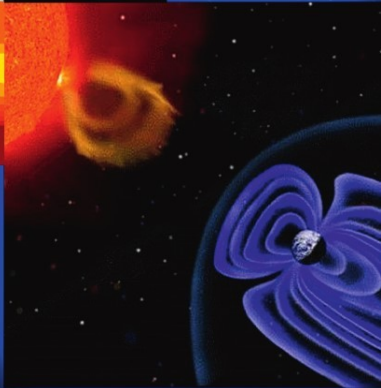
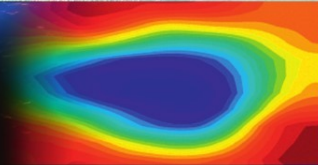
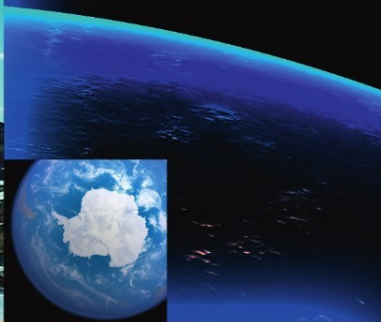


SPACE WEATHER MONITORING BY GROUND-BASED MEANS

PC index



Oleg Troshichev
& Alexander Janzhura

 Springer

PRAXIS

Space Weather Monitoring by Ground-Based Means

PC index

Oleg Troshichev and Alexander Janzhura

Space Weather Monitoring by Ground-Based Means

PC index



Published in association with
Praxis Publishing
Chichester, UK



Professor Oleg Troshichev
Arctic and Antarctic Research Institute
St. Petersburg
Russia

Dr Alexander Janzhura
Arctic and Antarctic Research Institute
St. Petersburg
Russia

SPRINGER-PRAXIS BOOKS IN ENVIRONMENTAL SCIENCES

ISBN 978-3-642-16802-4 e-ISBN 978-3-642-16803-1
DOI 10.1007/978-3-642-16803-1
Springer Heidelberg Dordrecht London New York

Library of Congress Control Number: 2011933665

© Springer-Verlag Berlin Heidelberg 2012

This work is subject to copyright, All rights are reserved, whether the whole or part of the material is concerned, specifically the rights of translation, reprinting, reuse off illustrations, recitation, broadcasting, reproduction on microfilm or in any other way, and storage in data banks. Duplication of this publication or parts thereof is permitted only under the provisions of the German Copyright Law of September 9, 1965, in its current version, and permission for use must always be obtained from Springer. Violations are liable to prosecution under the German Copyright Law.

The use of general descriptive names, registered names, trademarks, etc. in this publication does not imply, even in the absence of a specific statement, that such names are exempt from the relevant protective laws and regulations and therefore free for general use

Cover design: Jim Wilkie
Project copy editor: Rachael Wilkie
Typesetting: David Peduzzi

Printed on acid-free paper

Springer is a part of Springer Science+Business Media (www.springer.com)

Contents

List of figures	x
List of tables	xviii
List of abbreviations and acronyms	xix
About the authors	xxiii
1 Introduction	1
1.1 Reference	2
2 Physical background (historical outline)	3
2.1 Polar geomagnetic disturbances influenced by solar wind	3
2.2 Structure of electric fields in polar ionosphere.....	6
2.3 Magnetospheric field-aligned currents	8
2.4 Relation of field-aligned currents to aurora and particle precipitation.....	10
2.5 Model computations of field-aligned currents and ionospheric electric field and currents	12
2.6 Approaches to the idea of <i>PC</i> index.....	14
2.6.1 PC_L index	14
2.6.2 <i>MAGPC</i> index.....	14
2.7 Summary.....	16
2.8 References	16
3 A method for the <i>PC</i> index determination	23
3.1 Coefficients determining relationship between coupling function and magnetic activity	24
3.1.1 Level of reference for magnetic disturbance value δF	24
3.1.2 Direction of disturbance vectors and link between the δF and E_{KL} values	24

3.2	Calculation of the <i>PC</i> index	29
3.3	Interference of DP3 and DP4 disturbances	30
3.4	Verification of the derived <i>PC</i> indices	33
3.5	Physical meaning of the <i>PC</i> index	36
3.6	Summary	38
3.7	References	39
4	Special features of procedure for on-line <i>PC</i> index derivation	41
4.1	A need in producing 1-min <i>PC</i> index	41
4.2	Postulates used as a basis for the on-line <i>PC</i> index derivation	42
4.3	Derivation of quiet daily curve (QDC).....	44
4.3.1	Methods used to determine a level of reference and their inadequacy	44
4.3.2	Parameterization of geomagnetic variations for distinguishing quiet periods.....	46
4.3.3	A procedure for calculating a daily quiet curve (QDC)	46
4.3.4	Interpolation of a QDC for each day	48
4.3.5	Extrapolation of a QDC for subsequent days	51
4.3.6	Validity of the QDC derivation method.....	53
4.4	Allowance for IMF sector structure	56
4.4.1	Necessity of SS evaluation for QDC derivation	56
4.4.2	Separation of the sector structure effect in long series of observational data	58
4.4.3	On-line identification of the SS effect by ground magnetic data.....	61
4.5	Invariability of parameters α , β and ϕ in a solar activity cycle	66
4.5.1	The role of QDC in determination of parameters ϕ , α and β	66
4.5.2	Comparison of parameters α , β and ϕ calculated for solar maximum and minimum epochs	71
4.6	Summary.....	75
4.7	References	75
5	Solar wind–magnetosphere–ionosphere coupling and the <i>PC</i> index	77
5.1	Concepts of solar wind–magnetosphere coupling.....	77
5.1.1	Dungey’s concept of reconnection.....	77
5.1.2	Concept of ‘viscous-like’ interaction.....	80
5.1.3	Concept of magnetospheric plasma gradients as a driver for field-aligned currents	80
5.2	Solar wind–magnetosphere–ionosphere coupling and field-aligned currents	83
5.3	Solar wind–magnetosphere coupling functions.....	85
5.4	Saturation of cross-polar cap potential	87
5.5	<i>PC</i> index saturation	90
5.6	Summary.....	93
5.7	References	94

- 6 *PC* index response to solar wind geoeffective variations 103**
 - 6.1 *PC* index timing vs. interplanetary electric field variations 103
 - 6.2 Solar wind dynamic pressure variations 104
 - 6.2.1 Solar wind dynamic pressure impact on magnetospheric processes 104
 - 6.2.2 *PC* index timing vs. sudden changes in solar wind dynamic pressure 106
 - 6.2.3 Statistical relationships between the *PC* index and pressure pulses P_{sw} 108
 - 6.2.4 Relationships between *PC* and P_{sw} under conditions of negative pressure gradients and northward IMF 115
 - 6.3 Dynamics of the polar convection patterns related to solar wind pressure pulses 116
 - 6.4 Field-aligned currents determining the response of the *PC* index to solar wind pressure pulses 119
 - 6.5 Summary 126
 - 6.6 References 126

- 7 *PC* index as an indicator of substorm development 129**
 - 7.1 Previous analyzes of relations between polar cap magnetic activity and magnetosphere substorms 129
 - 7.2 Isolated substorms 130
 - 7.3 Periodically repetitive magnetic disturbances (sawtooth substorms) 140
 - 7.3.1 Definition of sawtooth substorms 140
 - 7.3.2 Examples of sawtooth magnetic disturbances 144
 - 7.3.3 Statistical relationship between *PC* (E_{KL}) variation and sawtooth magnetic disturbances development 148
 - 7.3.4 Evaluation of substorm back influence on polar cap magnetic activity 157
 - 7.4 *PC* index as a precursor of magnetic substorm development 158
 - 7.5 Threshold-dependent driven mode of magnetospheric substorms 162
 - 7.6 Summary 164
 - 7.7 References 165

- 8 *PC* index as an indicator of magnetic storm development 169**
 - 8.1 Identification of magnetic storms and separation of growth and decay parts in the main storm phase 169
 - 8.2 A *PC* index value required for the storm beginning 172
 - 8.3 Relationship between storm parameters and *PC* (E_{KL}) values 178
 - 8.4 ‘*Dst* index saturation’ and interplanetary electric field – magnetosphere coupling function 180
 - 8.5 Summary 184
 - 8.6 References 185

9	Specific features of magnetic disturbances occurring under conditions of a steadily high energy input into the magnetosphere	187
9.1	Inconsistency of substorm magnetic and aurora signatures in the case of powerful sawtooth substorms	187
9.2	Relationships between <i>PC</i> index and substorm (<i>AL</i>) and storm (<i>ASYM</i>) indices in conditions of the steadily high solar wind energy input into the magnetosphere	201
9.2.1	Existing ideas on interplay between magnetic storms and substorms	201
9.2.2	Relationships between <i>PC</i> , <i>AL</i> and <i>ASYM</i> indices for individual substorms	202
9.2.3	Relationships between <i>PC</i> , <i>AL</i> and <i>ASYM</i> indices during ‘ <i>PC</i> growth phase’ and ‘ <i>PC</i> decline phase’	206
9.2.4	A concept of powerful substorms reverse effect	213
9.3	Summary	215
9.4	References	216
10	Magnetic disturbances developing under conditions of northward IMF	219
10.1	Input of the IMF azimuthal component in coupling function E_{KL}	219
10.2	Magnetic storms developed under conditions of a northward IMF	221
10.3	Magnetospheric substorms developed under conditions of a northward IMF	221
10.4	Magnetospheric substorms triggered by sharp changes in the IMF vertical or azimuthal components	224
10.5	Summary	228
10.6	References	228
11	Causative discrepancies between summer and winter <i>PC</i> indices: physical implications	231
11.1	Reasons for discrepancy between summer and winter <i>PC</i> indices	231
11.2	Effects of IMF northward and azimuthal components	232
11.3	Effect of solar proton events	234
11.4	Effect of solar wind dynamic pressure pulses	236
11.5	Substorm development effect	237
11.6	Role of auroral ionosphere in supporting the magnetic activity in the winter polr cap	240
11.7	Statistical significance of <i>PC</i> seasonal differences	242
11.8	Summary	243
11.9	References	244

12 Monitoring of the auroral ionosphere 247

 12.1 Parameters characterizing an auroral ionosphere state..... 247

 12.2 Auroral absorption..... 248

 12.3 Ionospheric Es and F2 layers..... 253

 12.4 Summary..... 255

 12.5 References 255

13 PC index as indicator of anomalous atmospheric processes in the winter

Antarctica 257

 13.1 Solar activity influence on the Earth’s atmosphere: variations in
 cosmic rays flow or changes in solar wind parameters?.....257

 13.2 Distinctive features of atmospheric circulation over the winter
 Antarctica 261

 13.3 Cloudiness and sudden warmings in central Antarctica 265

 13.4 Changes in height profiles of temperature and pressure above Vostok
 station 268

 13.5 Anomalous winds at the Antarctic stations and their relation to the
 PC index 270

 13.6 Mechanisms suggested to explain solar wind influence on atmospheric
 processes..... 275

 13.7 Summary.....276

 13.8 References276

14 Conclusions..... 279

 14.1 References 281

Acknowledgements 283

Index..... 285

List of figures

Figure 2.1	Current systems of polar cap magnetic disturbances generated by southward ((a) and (b)), northward (c) and azimuthal (d) IMF components.	5
Figure 2.2	Current systems of residual polar cap magnetic disturbances unconnected with IMF.	6
Figure 2.3	Convection in the northern polar cap under various IMF orientations....	7
Figure 2.4	Pattern of field-aligned currents derived by Triad data.	9
Figure 2.5	Conformity of field-aligned currents with fluxes of auroral particle precipitation.	11
Figure 2.6	Current systems of polar cap magnetic disturbances derived from numerical simulations.	13
Figure 3.1	Equivalent current system of DP2 disturbances in summer (a) and winter (b) polar caps.	25
Figure 3.2	Direction of DP2 disturbance vectors at stations Vostok and Thule in various MLT hours.	27
Figure 3.3	Parameters α , β and ϕ determining link between coupling function E_{KL} and magnetic disturbance vectors at the Thule and Vostok stations.	28
Figure 3.4	Daily variation of α and β coefficient at Thule and Vostok designed for day of June 9.	30
Figure 3.5	Change of magnetic disturbance vectors δF at Thule and Vostok during June 9, 2001 and the appropriate PCN and PCS indices.	30
Figure 3.6	Average effect of azimuthal IMF component on convection patterns at Thule and Vostok.	32
Figure 3.7	Run of PCN and PCS indices in 1998–2001.	33
Figure 3.8	Behavior of differences $E_{KL}-PCN$ and $E_{KL}-PCS$ (in mV/m) during 2000.	34
Figure 3.9	Agreement between values $(E_{KL}-PCS)$ and $(E_{KL}-PCN)$	35
Figure 3.10	Careful and careless determination of the PCS index on example of April of 1997 and 1998.	35

Figure 3.11	Relation between PC index and ionospheric electric field measured by DMSP spacecraft.	37
Figure 4.1	A set of 1-minute quiet segments in H -component at Vostok used for calculation of QDC.	47
Figure 4.2	Run of H component at Vostok in June 2002 and an appropriate quiet daily variation.	49
Figure 4.3	Monthly averaged quiet daily variations calculated by the independent data sets for 2002.	49
Figure 4.4	Quiet daily variations in H and D components at Vostok station calculated for November in 1997 and 2002 and levels of QDC amplitudes during the Novembers of 1997–2002.	50
Figure 4.5	Comparison of QDC derived by extrapolation method with actual quiet daily variation for 12 September, 2002.	52
Figure 4.6	Standard deviations of differences between the mean daily values and the running 1-min H -component at the Vostok station and between the mean daily values and the QDC for 2002.	53
Figure 4.7	Run of H -component at the Vostok station during 5 international quiet days in June and November 2002 and the appropriate QDC.	54
Figure 4.8	Graphic presentation of QDC behavior for H and D components at Vostok in 1997–2001.	55
Figure 4.9	Standard deviations for differences between the actual QDC and ‘invariable’ QDC and between the actual QDC and ‘extrapolated’ QDC.	56
Figure 4.10	Actual run of 1-min H component at Thule during summer of 2001 and superposed quiet daily curve (QDC).	57
Figure 4.11	Original data series of azimuthal IMF component measured on board ACE spacecraft and SS effect displayed by the method of filtration.	59
Figure 4.12	Original data series of D and H components observed at the Thule station and SS effect displayed by the method of filtration.	59
Figure 4.13	Comparison between SS structures derived from spacecraft measurements and ground magnetic variations observed in H and D components at the Thule station.	60
Figure 4.14	Mean daily variation of H component at Thule derived for three gradations of azimuthal IMF component for summer months of 1998 and 2001.	61
Figure 4.15	Behavior of the H component median values at Thule during June months of 1998 and 2001 derived for time intervals of different duration (1, 3 and 5 days).	63
Figure 4.16	SS effects derived by H component observed at station Thule in 1998 and 2001 in comparison with actual variation of the IMF B_Y component measured by ACE spacecraft.	64
Figure 4.17	Relationship between the sector structure magnitudes derived from satellite-based and ground-based sets of data.	66
Figure 4.18	Daily variation of the angle ϕ and coefficients β and α derived respectively with inclusion of a QDC and without using a QDC.	67

Figure 4.19	<i>PCS</i> indices calculated with a QDC (PC_{QDC}) and without using a QDC (PC_0).	69
Figure 4.20	Seasonal variation of the differences between <i>PCS</i> values calculated with a QDC (PC_{QDC}) and without a QDC (PC_0) in 2002.	70
Figure 4.21	Variation of the QDC in the <i>H</i> component at Vostok station in November for the solar maximum (2002) and solar minimum (2007) epochs.	71
Figure 4.22	Parameters α , β and ϕ for the Vostok station, derived independently for epochs of solar maximum, solar minimum, and the full cycle of solar activity.	72
Figure 4.23	Indices $PC(solmax)$ and $PC(solmin)$ calculated for the same periods (December and June 2001) with use of two independent sets of parameters α , β and ϕ	73
Figure 5.1	Dungey's model of reconnecting interplanetary and geomagnetic fields.	82
Figure 5.2	The R1 and R2 FAC patterns mapped to equatorial plane with use of the Fairfield and Mead (1975) model of magnetic field (Potemra, 1978).	82
Figure 5.3	The R1 and R2 FAC patterns mapped to equatorial plane with use of the Tsyganenko (1996, 2002) models of magnetic field (Antonova <i>et al.</i> , 2006).	83
Figure 5.4	Normalized plasma pressure ∇p mapped to the equatorial plane (Wing and Newell, 2000).	84
Figure 5.5	Sources of particle precipitation in the dayside ionosphere identified by particle spectra (Newell and Meng, 1992).	84
Figure 5.6	Cross polar potential (PCP) versus interplanetary electric field (Kan <i>et al.</i> , 2010).	88
Figure 5.7	Cross polar potential and reverse convection potential as a function of interplanetary electric field (Sundberg <i>et al.</i> , 2009).	89
Figure 5.8	Relationship between the 1-min values of PCN/PCS indices and coupling function E_{KL} for summer seasons of 1998–2001.	91
Figure 5.9	Variations of coupling functions $E_{KL}(Em)$ and E_{K-R} (Kivelson and Ridley, 2008) and run of PC index in event of November 20, 2003 (Gao <i>et al.</i> , 2011).	91
Figure 5.10	Incidence of PC indices of different value.	92
Figure 6.1	Time changes of quantities E_{KL} and PCN for particular events with sharp rise and sharp decline of E_{KL} value (Stauning and Troshichev, 2008).	104
Figure 6.2	Timing and amplitudes of steep P_{sw} increases and related changes in PCN , the key date (T=0) being taken in different manner (Stauning and Troshichev, 2008)	107
Figure 6.3	Timing and amplitudes of steep P_{sw} increases and related changes in PCN for day and night hours at Thule (Stauning and Troshichev, 2008).	107
Figure 6.4	Behavior of average solar wind velocity v , dynamic pressure P_{sw} , and coupling function E_{KL} derived for 62 pressure jumps in 1998–2002... ..	109

Figure 6.5	Method used for automatic identification of the solar wind dynamic pressure sudden jump.	110
Figure 6.6	Relationship between averaged P_{SW} , E_{KL} and PC quantities under varying restrictions imposed on coupling function E_{KL}	111
Figure 6.7	Relationship between averaged P_{SW} , E_{KL} and PC quantities under varying restrictions imposed on the solar wind pressure value after the jump.	112
Figure 6.8	Relationship between averaged P_{SW} , E_{KL} and PC quantities under varying restrictions imposed on the pressure increase rate (dP/dt).	113
Figure 6.9	Relationship between averaged P_{SW} , E_{KL} and PC quantities under conditions of negative pressure gradient and northward IMF.	115
Figure 6.10	Patterns of equivalent ionospheric convection at the epoch time of $T=+6$ min in reference to SSC events (Stauning and Troshichev, 2008).	117
Figure 6.11	Polar convection patterns plotted for the epoch times from $T=-2$ min to $T=+3$ min in reference to SSC onsets (Stauning and Troshichev, 2008).	118
Figure 6.12	Field-aligned currents calculated for epoch time $T=0$ (Stauning and Troshichev, 2008)	120
Figure 6.13	Field-aligned currents calculated for epoch times of $T=5, 10, 15$ and 20 min (Stauning and Troshichev, 2008).	121
Figure 6.14	Displacement of convection vortex centers during period from $T=-1$ min to $T=+20$ min in reference to SSC onset (Stauning and Troshichev, 2008).	122
Figure 6.15	Development of FAC systems in magnetosphere following the solar wind pressure pulses impact on magnetosphere (Stauning and Troshichev, 2008).	123
Figure 7.1	Example of two magnetic bays developing on 27 February, 1998 against the background of magnetic quiescence.	131
Figure 7.2	Procedure used for identification of a magnetic substorms sudden onset.	132
Figure 7.3	Relationships between changes in the PC and AE indices for isolated magnetic bays.	133
Figure 7.4	Relationships between changes in the PC and AE indices for short isolated substorms.	134
Figure 7.5	Relationships between changes in the PC and AE indices for long isolated substorms.	135
Figure 7.6	Relationships between changes in the PC and AE indices for extended isolated disturbances.	136
Figure 7.7	Behavior of the averaged PC index in the summer and winter polar caps and the mean AL and AU indices derived for 4 classes of isolated magnetic disturbances.	138
Figure 7.8	Correlation between the AE and PC indices in the northern and southern polar caps during 1988–2001.	139

Figure 7.9	Identification of a <i>PC</i> growth beginning (<i>PC</i> increase), <i>AL</i> gradual growth beginning (<i>AL</i> increase) and <i>AL</i> explosive increase (<i>AL</i> sudden onset) adopted in the analysis.	141
Figure 7.10(a)	Sawtooth magnetic disturbances on August 28–29, 2000.	145
Figure 7.10(b)	Sawtooth magnetic disturbances on October 4, 2000.	146
Figure 7.10(c)	Saw-tooth magnetic disturbances on November 6, 2000.	147
Figure 7.11	Correlation between mean summer and winter <i>PC</i> indices over the growth phase (a) and in the expansion phase (b).	149
Figure 7.12	Relationships between mean variations of the IMF B_z and B_y components, coupling function E_{KL} , <i>PC</i> and <i>AL/AU</i> indices in case of sawtooth magnetic disturbances.	151
Figure 7.13	Delay times of <i>AL</i> gradual increase and <i>AL</i> sudden onset relative to <i>PC</i> growth beginning.	152
Figure 7.14	Correlation between sawtooth substorm intensity (<i>ALmax</i>) and <i>PC</i> index value for growth and expansion phases.	153
Figure 7.15	Delay time of <i>ALmax</i> vs. delay times of maximal polar cap magnetic activity (<i>PCmax</i>) in the summer (a) and winter (b) polar caps.....	154
Figure 7.16	Relationships between the growth phase duration (<i>Tgro</i>) and the <i>PCmean</i> value.	155
Figure 7.17	Relationship between the growth phase duration (<i>Tgro</i>) and the <i>PC</i> growth rate (PC_{GR}).	156
Figure 7.18	Ratios PC/E_{KL} and $PC*100/ AL $ for sawtooth magnetic disturbances.	157
Figure 7.19	Relationship between average <i>PC</i> and <i>AL</i> indices for weak magnetic bays, isolated short and extended substorms, and sawtooth substorms. ..	159
Figure 7.20	Dependence of <i>AL</i> growth rate and substorm intensity <i>ALmax</i> on <i>PC</i> growth rate.	161
Figure 8.1	Separation of growth and damping phases within the storm main phase.	171
Figure 8.2	Behavior of coupling function E_{KL} and <i>PC</i> index and respective <i>Dst</i> index variation for 8 storms of different intensity.	174
Figure 8.3	Relationship between behavior of averaged E_{KL} and <i>PC</i> index quantities and development of magnetic storm (<i>Dst</i> index) for 6 gradations of storm intensity.	177
Figure 8.4	Relationships between storm intensity <i>Dst(peak)</i> and quantities $E_{KL,growth}$ and PC_{growth} averaged over the storm growth phase interval.	179
Figure 8.5	Correlation between quantities ($Dst(trans_{E_{KL}})$) and ($Dst(trans_{PC})$)	181
Figure 8.6	Correlation between the storm parameter <i>Dst(trans)</i> and the storm intensity <i>Dst(peak)</i>	181
Figure 8.7	Relationships between the storm parameter <i>Dst(trans)</i> and the corresponding quantities $E_{KL}(damp)$ and $PC(damp)$ averaged over the storm damping phase interval.	182

Figure 8.8	Parameters Dst_{peak} and Dst_{trans} calculated as a function of PC index and coupling function E_{KL}	183
Figure 9.1	Patterns of ionospheric convection derived 2 min prior to and 2 min after the sawtooth substorm onset.	189
Figure 9.2	Sawtooth magnetic disturbances on October 4, 2000 and March 19–20, 2001.	190
Figure 9.3	The electron flux injections detected at the geosynchronous orbit on October 4, 2000 and March 19–20, 2001.	192
Figure 9.4	Sequence of aurora images for three substorms on October 4, 2000.	193
Figure 9.5	Sequence of aurora images for three substorms on March, 2001.	195
Figure 9.6	Time lags between aurora brightening and particle injections at geostationary orbit.	200
Figure 9.7	Relationship between PC , AL and $ASYM$ indices generalized over magnetic storms on October 4, 2000.	203
Figure 9.8	Relationships between PC , AL and $ASYM$ indices generalized over 9 storm events.	205
Figure 9.9	The generalized relationships between PC and $ASYM$, AL and $ASYM$ indices.	206
Figure 9.10	Run of AL , PC_{win} , PC_{sum} , and ASY indices superposed for 39 substorms with sudden onset ($SO=500$ nT) in course of PC growth and PC decline phases.	208
Figure 9.11	Relationships between the mean AL , PC , $ASYM$ indices for PC growth and PC decline phases.	209
Figure 9.12	Dependence of the AL drop and PC drop during the recovery phase on substorm intensity.	211
Figure 9.13	Dependence of the sawtooth substorm periodicity on average PC value and substorm intensity.	212
Figure 10.1	Relationship between coupling function E_{KL} and corresponding PC index under conditions of northward IMF $B_z > 2$ nT in respect to azimuthal IMF component (1998–2002).	220
Figure 10.2	Development of storm on January 21–22, 2005 under conditions of northward IMF.	222
Figure 10.3	Examples of three substorms developing under conditions of northward IMF.	223
Figure 10.4	Examples of substorms triggered by IMF northward turning or by sharp change of IMF B_y polarity.	225
Figure 10.5	Superposition of the IMF B_y and B_z components, PC and AL indices for 12 substorms related to IMF northward turning.	227
Figure 11.1	Example of asymmetrical response of summer and winter PC indices to impact of northward and azimuthal IMF components.	233
Figure 11.2	Sawtooth substorm on November 26–27, 2000 developed against the background of a solar proton event.	235
Figure 11.3	Behavior of the differences $(PC_{sum}-E_{KL})/E_{KL}$ and $(PC_{win}-E_{KL})/E_{KL}$ in reference to the sudden pressure jump moment.	236

Figure 11.4	Behavior of differences $(PC_{sum}-PC_{win})/PC_{win}$ for 3 categories of isolated disturbances in reference to the substorm sudden onset.	238
Figure 11.5	Scheme presenting the Region 1 currents closure in the summer and winter polar caps for magnetically quiet, weakly disturbed, and strongly disturbed conditions.	241
Figure 11.6	Statistically mean difference between values of summer and winter PC indices in 2000 as a function of the IMF B_z component.	242
Figure 12.1	Run of the PC index and development of auroral absorption on January 7, 2004.	249
Figure 12.2	Distribution of maximal absorption observed at the Canadian chain of stations under conditions of low magnetic activity.	250
Figure 12.3	Distribution of maximal absorption observed at the Canadian chain of stations under conditions of enhanced magnetic activity.	251
Figure 12.4	Correlation between the 1 min values of PC and absorption as a function of UT and geomagnetic latitude for winter months with low and enhanced magnetic activity.	251
Figure 12.5	Relationship between the PC index and auroral absorption at latitudes 63.9° and 68.7° derived for time intervals of their best correspondence.	252
Figure 12.6	Daily variations of parameters F_0E_s and f_0F_2 under quiet and disturbed conditions.	254
Figure 13.1	Relationship between average Forbush decrease (FD), southward IMF component (B_{zs}), and cloudiness above Vostok for the most powerful FD events.	258
Figure 13.2	Changes in daily mean cloudiness for three gradations of IMF B_{zs} component.	260
Figure 13.3	Drainage pattern of near-surface katabatic winds (Parish and Bromwich, 1991).	262
Figure 13.4	Conceptual scheme of vertical mass circulation forced by the katabatic wind regime in Antarctica (Parish and Bromwich, 1991). ...	263
Figure 13.5	Relationship between daily averaged PC index and cloudiness above the Vostok station in cases IMF strong negative and strong positive deviations of the IMF B_z component.	264
Figure 13.6	Relationship between PC index, IMF B_z component and sudden changes of surface temperature at Vostok in winter seasons of 1978–1992.	266
Figure 13.7	Hourly temperature changes ΔT at stations Vostok, Dome C, and South Pole as a function of number of hourly intervals with $B_z < -2$ nT.	267
Figure 13.8	Transformation of temperature height profiles above Vostok under conditions of positive and negative PC index deviations in 1978–1991.	269
Figure 13.9	Transformation of atmospheric pressure height profiles above Vostok under conditions of positive and negative PC index deviations in 1978–1991.	270

Figure 13.10	Relationship between daily averaged <i>PC</i> index, IMF B_z component and extended (~ 2 days) anomalous winds at the Vostok station during the winter seasons of 1981–1989.	271
Figure 13.11	Anomalous winds at stations Vostok, Neumayer, Casey and Russkaya in their relation to changes in the IMF B_z for winter seasons of 1981–1989.	272
Figure 13.12	Spatial distribution of regular and anomalous winds at the Antarctic stations.	273
Figure 13.13	Global atmospheric electric circuit and causes of its temporal and spatial variation (Tinsley and Zhou, 2006).	274

List of tables

Table 6.1	Average E_{KL} and PC values for different dynamic pressure gradients ΔP_{SW}	114
Table 7.1	Parameters of sawtooth substorms examined in the analysis: start of the PC growth, start of the AL growth and sudden onset of the AL increase.	143
Table 7.2	Mean values of PC and AE indices typical of different gradations of magnetic disturbances.	160
Table 8.1	List of magnetic storms used in the analysis.	170
Table 9.1	The onset times of magnetic disturbances, auroral brightenings and particle injections identified in the course of the repetitive bay-like disturbances on October 4, 2000, March 20, 2001, August 28–29, 2000, November 6, 2000, and November 27, 2000.....	198
Table 9.2	Maximal coefficients of correlation between PC and AL indices, between PC and $ASYM$ indices, and between AL and $ASYM$ indices with indication of corresponding delay times. Delay times of AL and $ASYM$ indices relative to PC are marked by (+), ahead times of AL relative to PC are marked by (–).	204
Table 12.1	List of stations whose riometer observations were used in the analysis.....	248

List of abbreviations and acronyms

AA	auroral absorption
AARI	Arctic and Antarctic Research Institute
AWS	automatic weather station
AE	index of magnetic activity in the auroral zone: $AE = AU + AL $
AL	index of negative magnetic activity in the auroral zone
ASYM	index characterizing asymmetry of DR disturbances
AU	index of positive magnetic activity in auroral zone
a_p	planetary geomagnetic activity index
BPS	boundary plasma sheet
BR	radiation balance
BY	field-aligned current system determined by the IMF B_y component impact on magnetosphere
B	magnitude of interplanetary magnetic field IMF
B_T	tangential IMF component in GSM coordinates: $B_T = (B_y^2 + B_z^2)^{1/2}$
B_x	radial IMF component in GSM coordinates
B_y	azimuthal IMF component in GSM coordinates
B_z	vertical IMF component in GSM coordinates
B_{ZN}	northward (positive) IMF component in GSM coordinates
B_{ZS}	southward (negative) IMF component in GSM coordinates
CCW	counterclockwise convection
CME	coronal mass ejection
CPCP	cross polar cap potential
CPCV	cross polar cap convection velocity
CPS	central plasma sheet
CW	clockwise convection
DCF	magnetic disturbances produced by currents flowing over the magnetopause
DMI	Danish Meteorological Institute
DPO	magnetic disturbances available irrespective of IMF impact on magnetosphere

DP1	magnetic disturbances of substorm type
DP2	high-latitude magnetic disturbances initiated by IMF B_{ZS} impact on magnetosphere
DP3	high-latitude magnetic disturbances initiated by IMF B_{ZN} impact on magnetosphere
DP4	high-latitude magnetic disturbances initiated by IMF B_Y impact on magnetosphere
DR	magnetic disturbances produced by ring current in the inner magnetosphere
Dst	index intensity of magnetic storms
E	electric field (interplanetary or ionospheric)
EDT	eccentric dipole time
E_{KL}	geoeffective interplanetary electric field determined by Kan and Lee (1979)
E_{KR}	geoeffective interplanetary electric field determined by Kivelson and Riedly (2008)
E_{SW}	interplanetary electric field bearing by solar wind
$E_T(E_Y)$	tangential component of interplanetary electric field
FAC	field-aligned currents
FD	Forbush decrease (of galactic cosmic rays flux)
f_0	critical frequency
GCR	galactic cosmic rays
HF	high frequency
$H,D,Z(X,Y,Z)$	components of geomagnetic field
IEF	interplanetary electric field
J(j)	electric currents (in ionosphere or magnetosphere)
K_p	planetary magnetic activity index
LLBL	low-latitude boundary layer
LT	local time
L-shell	radial distance in equatorial plane (in R_E) to the dipole magnetic line with certain value B
L1	Lagrange point
$l_0(l_{eff})$	stagnation (reconnection) line length
MHD	magneto-hydrodynamic (simulation)
MP	magnetopause
MAGPC	initial version of PC index
NBZ	field-aligned current system associated with the IMF B_{ZN} component impact on magnetosphere
Ne	electron density in the ionosphere layers
n	solar wind density
O^+	oxygen ions of ionospheric origin in the magnetosphere
PCA	polar cap absorption
PCP	cross polar potential
P_{sw}	solar wind dynamic pressure
PC	index of polar cap magnetic activity

<i>PCN</i>	index of polar cap magnetic activity in northern hemisphere
<i>PCS</i>	index of polar cap magnetic activity in southern hemisphere
<i>QDC</i>	quiet daily curve
R_E	the Earth's radius
Regions 1/2	main field-aligned currents systems in the magnetosphere
<i>SI</i>	sudden impulse
<i>SO</i>	(substorm) sudden onset
<i>SPE</i>	solar proton events
<i>SSC</i>	storm sudden commencement
S_q^p	quiet daily variation in the near-pole region
<i>SYM</i>	1-min index of the DR current intensity
<i>THL</i>	Thule station (Greenland)
<i>TCV</i>	traveling convection vortices
<i>UT</i>	universal (Greenwich) time
<i>UV</i>	ultra-violet irradiation
<i>VOS</i>	Vostok station (Antarctica)
<i>V</i>	geomagnetic field tube volume
V_A	Alfven velocity
$V_{sw}(v)$	solar wind velocity
α, β, ϕ	parameters characterizing statistically justified link between values δF and E_{KL}
$\delta F (\Delta F)$	value of the polar cap magnetic disturbance vector
ΔT	temperature gradient
ΔV	transpolar potential
θ	angle between the IMF B_T component and geomagnetic Z axis
Σ_A	Alfven conductivity
Σ_H	Hall conductivity
Σ_p	Pedersen conductivity
Φ_{PC}	$(\Delta\Phi)$ cross polar cap potential difference
Φ_{sw}	potential difference in solar wind

About the Authors

Oleg Troshichev

After graduating from the Faculty of Physics of Leningrad University (1961) and earning Ph.D degrees (1969) from the Siberian Institute of Earth Magnetism, Ionosphere, and Radiowave Propagation (Irkutsk), Oleg worked at Leningrad University. In 1978 he affiliated with the Arctic and Antarctic Research Institute (AARI). In 1979, he formulated the idea of polar cap magnetic activity as a proxy of the geoeffective solar wind influence on the magnetosphere. For over three decades he has led research programs that elaborate the procedures for the *PC* index derivation and methods for monitoring the magnetosphere state by means of the *PC* index. His contribution to solar–terrestrial physics includes: studies of the high-latitude magnetic disturbances and their relation to the field-aligned magnetospheric currents; elaboration of the mechanism for field-aligned current generation in the magnetosphere; the concept of solar wind influence on processes in the Antarctic winter atmosphere; mechanisms for the QBO influence on ozone content in polar caps, and others.

Alexander Janzhura

Alexander received his M.Sc from the Russian State Hydrometeorological University, St. Petersburg as master of science in 2002. From 1994 to 1998 he worked at the Russian Hydromet service stations in Arctica. In 1999, he affiliated with the Department of Geophysics of the Arctic and Antarctic Research Institute (AARI) in St. Petersburg, where he became a leading developer of hard- and software for geophysical research. He initiated the adoption of the digital data acquisition system for the Russian Arctic and Antarctic geophysical networks and organized the on-line transmission of geophysical data from remote stations to AARI. He played a crucial role in developing the on-line procedure for the *PC* index calculation. In 2009, he received his Ph.D degree in geophysic sciences. His thesis contained strong evidence that the *PC* index can be regarded as an adequate ground-based indicator of the solar wind energy that enters into the magnetosphere.

1. Introduction

The term ‘space weather’ came into being about 25–30 years ago to denote, by analogy with ‘meteorological weather’, a complex process of space phenomena and processes affected by varying sun activity. In its broad sense, the term refers to entire an heliosphere whose limits are determined by expanding fluxes of solar plasma. In its narrow, usual sense, the term applies to the Earth environment and, to be more exact, to the space subjected to geomagnetic field influence, i.e. to the Earth’s magnetosphere.

The concept of bad (disturbed) space weather covers a wide range of phenomena directly affecting human activity. They include satellite damage, radiation hazards for astronauts and airline passengers, telecommunication problems, outages of power and electronic systems, effects in the atmospheric processes, and even some evidence of impact on human health. These issues, as well as a description of some main physics processes that provide a basis of the above phenomena are well presented in the book *Space Weather: Physics and Effects* by Bothmer and Daglis (2007). Results highlighted in the book demonstrate the vital necessity of space weather forecasting and nowcasting. Prediction of space weather is based on continuous ground-based or space missions-based visual and instrumental observations of processes on the solar disc, primarily Coronal Mass Ejections (CME), that provide information on probable space weather disturbances 1–3 days in advance. Space weather nowcasting is based mainly on measurements of solar wind parameters – wind speed and IMF B_z component being the most important of them – at the Lagrange point L1, that provide information on predictable space weather changes about one hour in advance. Unfortunately, specific features of solar wind impact on the Earth’s magnetosphere imperfectly and so never conform to solar wind features detected at point L1, except interplanetary shocks producing powerful magnetic disturbances.

Taking into account extremely vague ideas on the physical mechanisms of the solar wind–magnetosphere coupling and a lack of regular information on the magnetopause parameters in their relation to the solar wind impact, it would be very important to derive an adequate indicator displaying the coupling efficiency, using regular observations within the magnetosphere. It is becoming obvious right away that satellites moving in space cannot provide timely data on plasma and magnetic fields at the required points of the magnetosphere; in addition, there is always a problem of separation of temporal and spatial varia-

tions in spacecraft device readings. It implies that a ground network of observations must form the basis for a derivation of a coupling efficiency indicator with reference to satellite-based measurements to testify and verify the indicator.

Indeed, ground-based indices such as Kp , AE and Dst (we shall not mention other less popular ones), are commonly considered as indicators displaying the power of disturbances in the magnetosphere and, therefore, the current state of space weather. However, all these indices characterize the energy realized in the form of magnetospheric disturbances but not the energy coming into the magnetosphere, or that stored in the magnetosphere, while coupling the solar wind with the magnetosphere. Indeed, the AE index, which is regarded as a characteristic of a magnetospheric substorm, is a measure of electrojet intensity in the auroral zone; the Dst index, regarded as a characteristic of global magnetospheric storms, is a measure of magnetic depression in the H component in the equatorial zone; and the physical meaning of the Kp index is not clear at all. So all these indices do not display a solar wind energy input into the magnetosphere, and therefore cannot be regarded as an indicator of the efficiency of solar wind–magnetosphere coupling. Only coupling efficiency monitoring is important for reliable space weather nowcasting.

This monograph is devoted to the PC index which was put into practice about 30 years ago as an index of polar cap magnetic activity. Some recent studies have showed that the implications of a PC index seem to be far more significant: the index can be considered as an adequate proxy of solar wind energy incoming into the magnetosphere, and a basic procedure for PC index calculation has been developed to provide uninterrupted on-line PC index derivation. These circumstances make it possible to examine the PC index as the most proper applicant to monitor the geoefficiency of the solar wind–magnetosphere coupling, and therefore to monitor (and nowcast) space weather changes.

The following issues are discussed in the book:

- PC index concept;
- PC index derivation procedure and its verification;
- PC index response to solar wind parameters changes;
- PC index relation to magnetospheric substorms and magnetic storms;
- PC index saturation and solar wind–magnetosphere coupling functions, physical sense of occasional discrepancies between summer and winter indices;
- PC index as an indicator of an auroral ionosphere state and anomalous atmospheric processes in Antarctica; and
- physical meanings of some peculiarities in PC index behavior

1.1 Reference

Bothmer V, Daglis IA (2007) Space weather: physics and effects. Chichester: Springer Praxis

2. Physical background (historical outline)

2.1 Polar geomagnetic disturbances influenced by solar wind

The first examinations of the relations between solar wind variations and geomagnetic activity, represented by the Kp index, displayed the dependence of the Kp value on the solar wind speed v and the interplanetary magnetic field (IMF) intensity B (Coleman *et al.*, 1961; Snyder *et al.*, 1963). Later, it was found that magnetic activity is much better determined by the IMF southward (B_{zs}) component (Fairfield and Cahill, 1966; Wilcox *et al.*, 1967; Rostoker and Fälthammar, 1967), or by the IMF transverse fluctuations $(\delta B_T)^2 = (\delta B_z)^2 + (\delta B_y)^2$ (Baliff *et al.*, 1967). The dependence of the auroral AE index on southward IMF was shown by Pudovkin *et al.* (1970), Arnoldy (1971), Foster *et al.* (1971), Kokubun (1972) and Meng *et al.* (1973). It was found that magnetic activity in the auroral zone starts to increase about 15–30 minutes after the IMF turns south, and the correlation between B_z and AE variations is maximal for the delay time ~ 40 minutes. As analyzes (Kokubun, 1972; Kane, 1974) showed, geomagnetic storms are also affected by the IMF southward component, but they develop only if the magnetosphere is exposed to the southward IMF for some hours. According to Hirshberg and Colburn (1969) and Russel *et al.* (1974), Dst variation develops when the value of southward IMF exceeds the threshold level of $-(3-5)$ nT. The correlation of the AE index with the solar wind fluctuations distinctly increases if the product of the solar wind speed and southward IMF is taken into account (Rostoker and Fälthammar, 1967; Garrett *et al.*, 1974; Murayama and Hakamada, 1975). The conclusion made by Rostoker and Fälthammar (1967) is that the interplanetary electric field $E = [vB_{zs}]$ plays a crucial part in geomagnetic disturbances.

The actual distribution of magnetic disturbances at ground level is commonly described by systems of equivalent currents being hypothetic currents, providing the observed magnetic effect on the ground surface. Nagata and Kokubun (1962) were the first to examine under the name of S_p^q a current system of high-latitude magnetic variations observed within the polar cap in periods free of magnetic disturbances. Next, Obayashi (1967) separated a special class of magnetic disturbances (DP2) from magnetic substorms (DP1): the DP2 current system consists of two vortices without any peculiarities in the auroral zone and with currents flowing sunward in the near-pole region. DP2 variations were extensively studied

by Nishida, who revealed their close relation to southward IMF (Nishida, 1968a,b; Nishida and Maezawa, 1971). According to Nishida (1968a), a DP2 currents system is a global system expanding from pole to equator, with focuses located at the latitudes of $\Phi=72-74^\circ$. Further studies (Troshichev, 1975) showed that a two-vortices DP2 current system is terminated by the latitudes of $\Phi=50-60^\circ$, the disturbances at the lower latitudes of $\Phi < 50^\circ$ being produced by equivalent zonal currents of the extra-ionospheric origin. Current vortices focuses in system (Troshichev, 1975) turned out to be located at the morning and evening poleward boundaries of the auroral oval ($\Phi=76-78^\circ$). This peculiarity made it possible to further identify the current vortices focuses with disposition of the magnetospheric field-aligned currents flowing in and out of the polar ionosphere. Kuznetsov and Troshichev (1977) also noted that variations similar to DP2 are observed in the absence of southward IMF. This fact has been attributed to the permanent availability of the geomagnetic variation of (S_p^a) type (Nagata and Kokubun, 1962). Similar permanent disturbances were also separated by Mishin *et al.* (1978) and Levitin *et al.* (1982). To explain generation of these weak disturbances, a mechanism of quasi-viscous interaction between the solar wind and the magnetosphere (Axford, 1964) was accepted.

Besides the DP2 currents affected by southward IMF, some other types of disturbances are also typical of the polar caps. An abnormal 'near-pole DP variation' with direction of currents opposite to that in DP2 was separated by Iwasaki (1971) in the dayside summer polar cap. It was shown by Maezawa (1976) and Kuznetsov and Troshichev (1977) that these disturbances (named as DP3 by Kuznetsov and Troshichev (1977)) are observed when northward IMF impacts on the magnetosphere, and their current system consists of two less-scale current cells centered at latitudes of $\phi \sim 82^\circ$ with the current flow opposite to that in DP2.

Disturbances related to azimuthal IMF component were first separated as an effect of the IMF sector structure (Svalgaard, 1968; Mansurov, 1969). Later, their dependence on azimuthal IMF component was demonstrated (Friis-Christensen *et al.*, 1972; Sumaruk and Feldstein, 1973; Mishin *et al.*, 1973). The current system of these disturbances, named as BY or as DP4 (Kuznetsov and Troshichev, 1977), includes currents flowing along geomagnetic latitudes with maximal intensity in the daytime cusp region ($\Phi \sim 80^\circ$), the current direction being dependent on the sign of the IMF azimuthal component. The actual interplanetary magnetic field usually contains both vertical and azimuthal components, and the ground magnetic disturbances display the combined effect of DP2+DP4 or DP3+DP4 current systems. In these conditions, the influence of the azimuthal IMF component reveals itself in the deformation of the DP2 (or DP3) current systems: in the northern polar cap, the evening DP2 current vortex expands into the dawn sector under conditions of $B_Y > 0$, and the morning vortex expands into the dusk sector under conditions of $B_Y < 0$ (Matsushita *et al.*, 1973).

The multi-functional analysis of relationships between the IMF and geomagnetic components has been fulfilled by Troshichev and Tsyganenko (1979) to separate effects of the IMF B_x , B_y , B_z components in the case of their combined influence. Results of this analysis (presented in [Figure 2.1](#)) demonstrate, as in previous studies, availability of the DP2, DP3 and DP4 current systems associated with the action of southward, northward and azimuthal IMF components respectively. DP2 currents are shown in [Figure 2.1](#) for two different IMF B_{zs} values: $B_z = -1\text{nT}$ (left) and $B_z = -0.25\text{nT}$ (right). DP4 currents are shown for $B_Y > 0$ in

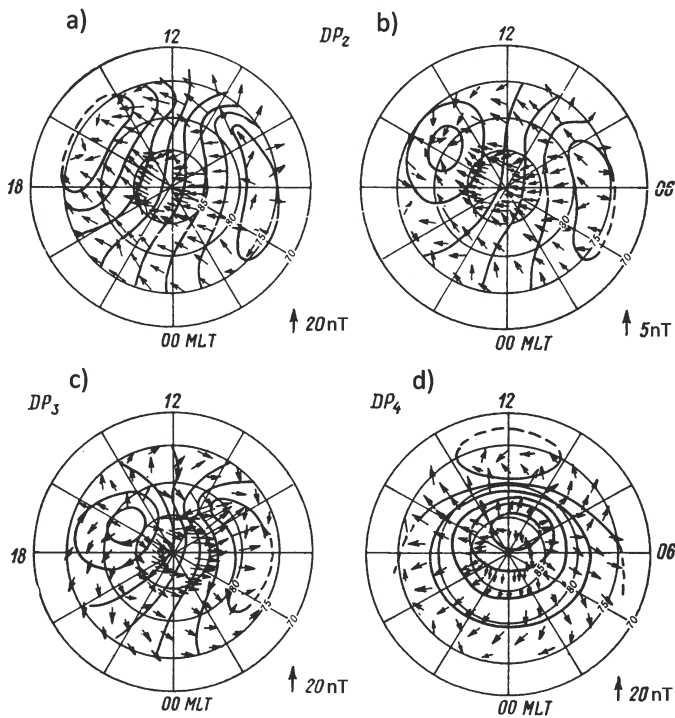


Figure 2.1 Current systems of DP2, DP3 and DP4 disturbances generated by variations of IMF components: (a) southward $B_{ZS} = -1 \text{ nT}$, (b) southward $B_{ZS} = -0.25 \text{ nT}$, (c) northward B_{ZN} , (d) azimuthal B_Y (Kuznetsov and Troshichev, 1977). Short arrows present distribution of the magnetic disturbance vectors on the ground surface.

the northern hemisphere. The current flow in DP4 system is quite opposite in the southern polar cap.

In addition, the residual magnetic disturbance DP0 unrelated to the IMF has been separated in line with the conclusion made by Kuznetsov and Troshichev (1977). The DP0 current system shown in Figure 2.2 for conditions of (a) northward and (b) southward IMF component is similar to the DP2 system, but exists permanently irrespective of the IMF polarity. Therefore, under the influence of southward IMF, the DP2 currents can be considered as an enhancement of currents in the constantly existing DP0 system. Later, Sergeev and Kuznetsov (1981) showed that intensity of the DP0 currents well correlates with the solar wind velocity v in the second power and, therefore, can be associated with the solar wind dynamic pressure.